

## Article

# New Low-Dimensional Hybrid Perovskitoids Based on Lead Bromide with Organic Cations from Charge-Transfer Complexes

Igor A. Nikovskiy <sup>1</sup>, Kseniya L. Isakovskaya <sup>1,2</sup> and Yulia V. Nelyubina <sup>1,\*</sup>

<sup>1</sup> A.N. Nesmeyanov Institute of Organoelement Compounds, Russian Academy of Sciences, Vavilova Str., 28, 119991 Moscow, Russia; igornikovskiy@mail.ru (I.A.N.); isakovskaia10@gmail.com (K.L.I.)

<sup>2</sup> Mendeleev University of Chemical Technology of Russia, Miusskaya pl., 9, 125047 Moscow, Russia

\* Correspondence: unelya@ineos.ac.ru

**Abstract:** We have obtained a series of low-dimensional hybrid perovskitoids (often referred to as perovskites) based on lead bromide. As organic cations, the derivatives of polyaromatic and conjugated molecules, such as anthracene, pyrene and (E)-stilbene, were chosen to form charge-transfer complexes with various organic acceptors for use as highly tunable components of hybrid perovskite solar cells. X-ray diffraction analysis showed these crystalline materials to be new 1D- and pseudo-layered 0D-perovskitoids with lead bromide octahedra featuring different sharing modes, such as in unusual mini-rods of four face- and edge-shared octahedra. Thanks to the low dimensionality, they can be of use in another type of optoelectronic device, photodetectors.

**Keywords:** lead bromide; low-dimensional perovskites; hybrid perovskites; charge-transfer complexes; perovskitoids; solar cells; X-ray diffraction



**Citation:** Nikovskiy, I.A.; Isakovskaya, K.L.; Nelyubina, Y.V. New Low-Dimensional Hybrid Perovskitoids Based on Lead Bromide with Organic Cations from Charge-Transfer Complexes. *Crystals* **2021**, *11*, 1424. <https://doi.org/10.3390/cryst11111424>

Academic Editors: Binbin Luo, Ruosheng Zeng and Feiming Li

Received: 10 November 2021  
Accepted: 18 November 2021  
Published: 21 November 2021

**Publisher's Note:** MDPI stays neutral with regard to jurisdictional claims in published maps and institutional affiliations.



**Copyright:** © 2021 by the authors. Licensee MDPI, Basel, Switzerland. This article is an open access article distributed under the terms and conditions of the Creative Commons Attribution (CC BY) license (<https://creativecommons.org/licenses/by/4.0/>).

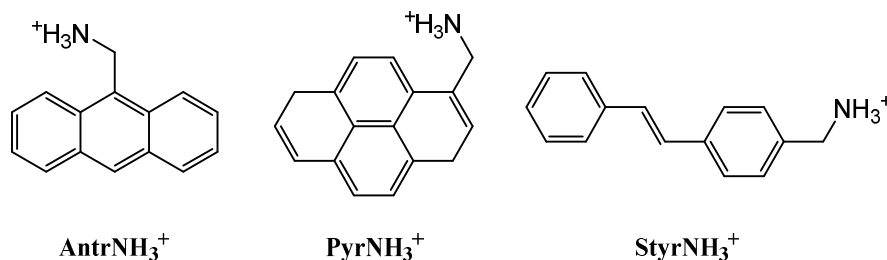
## 1. Introduction

Solar cells made with hybrid perovskite semiconductors [1] are believed to have a potential to revolutionize the field of renewable energy sources. These crystalline materials of the general formula  $AMX_3$  feature a three-dimensional periodic array of corner-sharing  $MX_6$  octahedra, where M is a large divalent metal ion (most often,  $Pb^{2+}$ ) and X is a halide anion ( $I^-$ ,  $Br^-$  or  $Cl^-$ ), with voids filled by organic cations A, such as methylammonium or formamidinium. Owing to an ability to produce high-quality single crystals and films with tunable optoelectronic characteristics [2], the hybrid perovskites are superior to crystalline silicon, a popular component of solar cells. They, however, suffer from low stability [3] and soon degrade when exposed to oxygen, moisture, heat and even sunlight.

As a solution [4,5], low-dimensional hybrid perovskites [3] were proposed in which  $MX_6$  octahedra or  $MX_5$  pyramids [6] are corner-shared in less than three dimensions. A wider choice of organic cations [7], which no longer have to meet strict size requirements [8,9], allows obtaining 2D- [10], 1D- [11,12] or 0D- [13] hybrid perovskites with promising optoelectronic properties. To further improve their performance in solar cells [14], inert organic cations are sometimes replaced [15] by electroactive molecules [16–20], including those encountered in organic charge-transfer complexes [18,21–24]. The latter may potentially provide additional functionalities to hybrid perovskites [25], such as (super)conductivity, photoconductivity, ferroelectricity and magnetoresistance [26,27] useful for optoelectronic devices [28]. An advantage of such organo-inorganic materials is the possibility to fine-tune their optoelectronic properties by using a proper combination of organic donors and acceptors [26,27] able to form a charge-transfer complex, which widens even further the opportunities for designing low-dimensional hybrid perovskites for various applications.

In this work, we synthesized a series of hydrobromides from previously reported [29–32] methanamine derivatives of anthracene, pyrene and (E)-stilbene, the popular donors

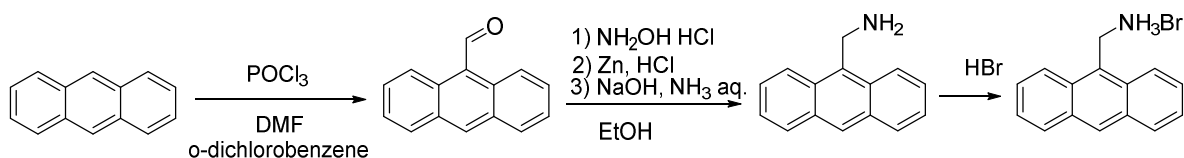
from charge-transfer complexes [26]. The corresponding cations (Scheme 1) have an alkylammonium group to bind the inorganic component of a hybrid perovskite via strong hydrogen bonds and a polyaromatic or conjugated core, to form a charge-transfer complex with an organic acceptor [26,27], such as tetracyanoethylene (TCNE). Their subsequent reaction with lead bromide in dimethylformamide, which provides a good solubility of both organic and inorganic compounds of our choice [21,22,33], resulted in new representatives of largely unexplored 0D- [6] and 1D-hybrid perovskites [11,21,34] or perovskitoids [35] with electroactive organic cations, as identified by X-ray diffraction analysis.



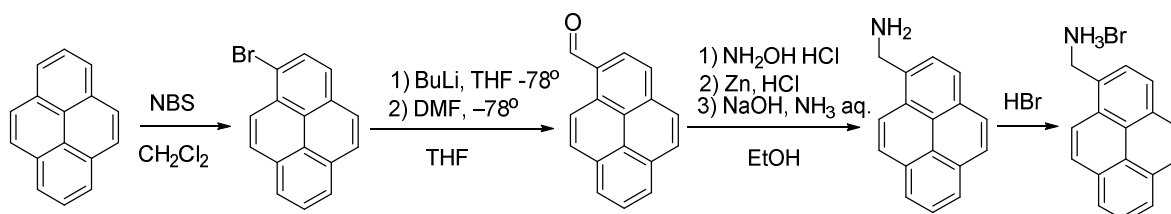
**Scheme 1.** Organic cations in this study: anthracen-9-ylmethanamonium, AntrNH<sub>3</sub><sup>+</sup>, pyren-4-ylmethanamonium, PyrNH<sub>3</sub><sup>+</sup>, and (E)-(4-styrylphenyl)methanamonium, StyrNH<sub>3</sub><sup>+</sup>.

## 2. Materials and Methods

**Synthesis.** All synthetic manipulations were carried out on air unless stated otherwise. Solvents were purchased from commercial sources and purified by distilling from conventional drying agents under an argon atmosphere prior to use. Anthracene, pyrene and styrene were obtained commercially (Sigma-Aldrich). The 9-Anthracenecarboxaldehyde [36], 1-bromopyrene [37], 1-pyrenecarbaldehyde [38] and (E)-4-styrylbenzaldehyde [39] were synthesized as reported earlier, while the corresponding hydrobromides, as described in [40] (Schemes 2–4). <sup>1</sup>H spectra were recorded from solutions in DMSO-d<sub>6</sub> or CDCl<sub>3</sub> with Varian 400 Inova FT-spectrometer (Varian, Palo Alto, Santa Clara, CA, USA) with 400.13 MHz <sup>1</sup>H frequency; the measurements were done using the residual signals of these solvents (<sup>1</sup>H 2.50 ppm and 7.26 ppm).



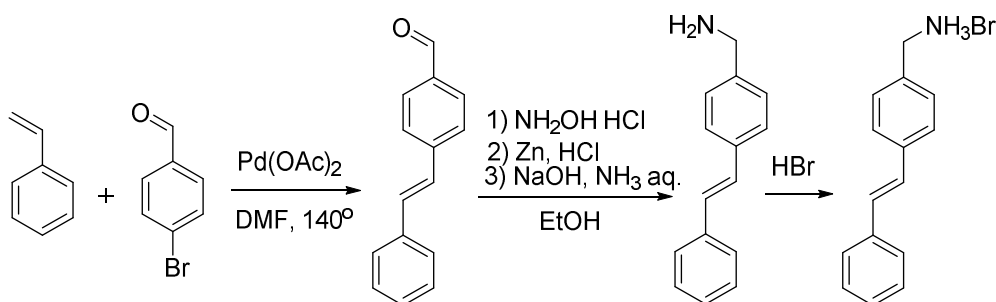
**Scheme 2.** Synthesis of anthracen-9-ylmethanamonium hydrobromide, AntrNH<sub>3</sub>Br.



**Scheme 3.** Synthesis of pyren-4-ylmethanamonium hydrobromide, PyrNH<sub>3</sub>Br.

**Synthesis of 9-anthracenecarboxaldehyde (Scheme 2) [36].** In a 500 mL round-bottomed flask fitted with a magnetic stir bar and reflux condenser, phosphorus oxychloride (17.5 g, 0.115 mol) and anthracene (11.25 g, 0.065 mol) were mixed with 10 mL of o-dichlorobenzene in 200 mL of DMF. The flask was heated while stirring to 90–95 °C over a period of 30 min to give a deep red solution, which was heated for 3 h and then cooled to room temperature. Upon cooling, the residual reddish oil solidified. A solution of 70 g of

crystalline sodium acetate in 125 mL of water was then added to the cooled solution. The aqueous liquor was decanted. A crude solid was recrystallized from 50 mL of hot glacial acetic acid; when cold, the bright yellow aldehyde was filtered by suction, washed on the filter with 30 mL of methanol and dried in vacuum (10 mm Hg). Yield: 9.65 g (72%).  $^1\text{H}$  NMR ( $\text{CDCl}_3$ , 400 MHz, 293 K):  $\delta$ (ppm) = 11.45 (s., 1H, CHO), 8.93 (d.,  $^3J_{\text{H,H}} = 7.7$  Hz, 2H, 1- and 8-Antr-H), 8.59 (s., 1H, 10-Antr-H), 7.99 (d.,  $^3J_{\text{H,H}} = 8.85$  Hz, 2H, 4- and 5-Antr-H), 7.64 (t.,  $^3J_{\text{H,H}} = 7.7$ , 2H, 2- and 7-Antr-H), 7.51 (t.,  $^3J_{\text{H,H}} = 8.85$ , 2H, 3- and 6-Antr-H).



**Scheme 4.** Synthesis of (E)-(4-styrylphenyl)methanamonium hydrobromide, Styr  $\text{NH}_3\text{Br}$ .

**Synthesis of 1-bromopyrene (Scheme 3) [37].** In a 250 mL round-bottomed flask fitted with a magnetic stir bar, pyrene (5 g, 0.024 mol) and N-bromosuccinimide (4.4 g, 0.024 mol) were mixed in 100 mL of dichloromethane. The resulting suspension was stirred for 12 h at room temperature and then filtered while discarding the solid. The mother liquor was evaporated, and a crude solid was recrystallized from hot petroleum ether; when cold, white crystals of 1-bromopyrene were filtered by suction and dried in vacuum (10 mm Hg). Yield: 4.69 g (68%).  $^1\text{H}$  NMR ( $\text{CDCl}_3$ , 400 MHz, 293 K):  $\delta$ (ppm) = 8.43 (d,  $^3J_{\text{H,H}} = 9.2$  Hz, 1H, 7-Pyr-H), 8.20–8.24 (m, 3H, 2-, 4- and 6-Pyr-H), 8.17 (d,  $^3J_{\text{H,H}} = 9.2$  Hz, 1H, 8-Pyr-H), 8.09 (d,  $^3J_{\text{H,H}} = 8.9$  Hz, 1H, 5-Pyr-H), 7.99–8.06 (m, 3H, 3-, 9- and 10-Pyr-H).

**Synthesis of 1-pyrenecarbaldehyde (Scheme 3) [38].** 1-Bromopyrene (4 g, 0.014 mol, 1.0 equiv.) was put into a 250 mL one-necked round-bottomed Schlenk flask with a rubber septum equipped with a magnetic stir bar. The flask was evacuated under vacuum (10 mm Hg) and purged with nitrogen (three times). Dry THF (100 mL) was added in a nitrogen atmosphere. After cooling to  $-78$  °C, n-BuLi (2.5 M in hexane, 7.28 mL, 0.018 mol, 1.3 equiv.) was added via a syringe over a period of 10 min to produce a light-brown solution. After stirring for 15 min, anhydrous DMF (1.4 mL, 0.018 mol, 1.3 equiv.) was also added via a syringe, and the mixture was allowed to reach room temperature while stirring for 12 h overnight. When cooled, it was carefully poured into rapidly stirred water (100 mL), and diethyl ether (100 mL) was then added. The organic phase was separated and washed with water. After drying over  $\text{MgSO}_4$ , the mixture was filtered and the solvent was removed from the filtrate by rotary evaporation to produce an orange solid, which was then recrystallized from hot ethanol as yellow crystals. Yield: 2.06 g (64%).  $^1\text{H}$  NMR ( $\text{CDCl}_3$ , 400 MHz, 293 K):  $\delta$ (ppm) = 10.77 (s., 1H, CHO), 9.41 (d.,  $^3J_{\text{H,H}} = 9.3$  Hz, 1H, 7-Phen), 8.44 (d.,  $^3J_{\text{H,H}} = 8.0$  Hz, 1H, 2-Phen), 8.30 (t.,  $^3J_{\text{H,H}} = 7.5$  Hz, 3H, 4-, 6- and 8-Phen), 8.24 (t.,  $^3J_{\text{H,H}} = 9.3$  Hz, 2H, 3- and 5-Phen), 8.11–8.07 (m, 2H, 8- and 9-Phen).

**Synthesis of (E)-4-styrylbenzaldehyde (Scheme 4) [39].** An oven-dried 350-mL Schlenk flask was charged under nitrogen with  $\text{Cs}_2\text{CO}_3$  (12.32 g, 0.0378 mol) and DMF (100 mL). 4-Bromobenzaldehyde (5 g, 0.027 mol) and freshly distilled styrene (3.72 mL, 0.032 mol) were added via syringes.  $\text{Pd}(\text{OAc})_2$  (5 mg, 0.022 mmol) in DMF (1 mL) was then added via a syringe. The Schlenk tube was sealed under argon and placed in an oil bath preheated to 140 °C. At this temperature, the reaction mixture was stirred for 19 h. When cooled to room temperature, the reaction mixture was poured into water (250 mL) and extracted with dichloromethane. The organic extract was washed with brine, dried over  $\text{MgSO}_4$  and concentrated to dryness under vacuum (10 mm Hg). A crude product was purified by flash chromatography on silica (dichloromethane). Yield: 4.94 g (88%).  $^1\text{H}$  NMR

(CDCl<sub>3</sub>, 400 MHz, 293 K):  $\delta$ (ppm) = 9.98 (s, 1H, CHO), 7.80 (2H,  $^3J_{H,H}$  = 8.0 Hz, 3-PhCHO), 7.57 (d, 2H,  $^3J_{H,H}$  = 8.0 Hz, 2-PhCHO), 7.49 (t, 2H,  $^3J_{H,H}$  = 8.0 Hz, m-Ph), 7.41–7.21 (m, 5H, o-Ph, p-Ph, CH=CH).

**General procedure for the preparation of amine hydrobromides (Schemes 2–4) [40].** A solution of an appropriate aldehyde (12.25 mmol, 1 equiv.) and hydroxy-ammonium chloride (1.025 g, 14.7 mmol, 1.2 equiv.) in ethanol (80 mL) was stirred for 1 h. Then, hydrochloric acid (12 M, 4.08 mL, 4 equiv.) and zinc dust (2 g, 30.63 mmol, 2.5 equiv.) were slowly added, and the resulting mixture was stirred at room temperature for 45 min. A solution of ammonia (30%, 3.5 mL) and sodium hydroxide (6 M, 7.5 mL) was added dropwise. The mixture was stirred at room temperature for 15 min and then filtered; the solid was discarded and the mother liquor, poured into water (100 mL). The resulting suspension was extracted with dichloromethane, dried over anhydrous sodium sulfate and filtered. The solvent was removed under vacuum (10 mm Hg) to produce a solid residue that was suspended in aqueous HBr (48%) and stirred for 5 min, filtered and washed with water until the pH values reaches 7. The solid was then dried in high vacuum (1 mm Hg) and used without further purification.

**Anthracen-9-ylmethanamine hydrobromide.** Yield: 1.44 g (41%). <sup>1</sup>H NMR (DMSO-d<sub>6</sub>, 400 MHz, 293 K):  $\delta$ (ppm) = 8.62 (s, 1H, 10-Antr), 8.43 (d.,  $^3J_{H,H}$  = 8.8 Hz, 2H, 4- and 5-Antr), 8.12 (d, 2H,  $^3J_{H,H}$  = 8.3 Hz, 1- and 8-Antr) 7.62 (t,  $^3J_{H,H}$  = 8.8 Hz, 2H, 3- and 6-Antr), 7.55 (t.,  $^3J_{H,H}$  = 8.3 Hz, 2H, 2- and 7-Antr), 4.84 (br.s., 2H, CH<sub>2</sub>NH<sub>2</sub>).

**Pyren-4-ylmethanamine hydrobromide.** Yield: 1.18 g (31%). <sup>1</sup>H NMR (CDCl<sub>3</sub>, 400 MHz, 293 K):  $\delta$ (ppm) = 8.49–8.32 (m., 4H, Pyr), 8.26–8.20 (m., 4H, Pyr) 8.12 (t, 1H, Pyr) 4.83 (d.,  $^3J_{H,H}$  = 5.0 Hz, 2H, CH<sub>2</sub>NH<sub>2</sub>).

**(E)-(4-styrylphenyl)methanamine hydrobromide.** Yield: 1.5 g (45%). <sup>1</sup>H NMR (CDCl<sub>3</sub>, 400 MHz, 293 K):  $\delta$ (ppm) = 7.65–7.58 (m., 4H, PhNH<sub>2</sub>), 7.47–7.31 (m., 5H, Ph), 3.85 (s., 2H, CH<sub>2</sub>NH<sub>2</sub>).

**Synthesis of [AntrNH<sub>3</sub>][PbBr<sub>3</sub>](DMF).** In a 5 mL scintillation vial filled with 2 mL of DMF, anthracen-9-ylmethanamine hydrobromide (10 mg, 0.0347 mmol) was mixed with PbBr<sub>2</sub> (12.7 mg, 0.0347 mmol) and tetracyanoethylene (4.4 mg, 0.0347 mmol). The resulting suspension was heated until the mixture became clear. After cooling to room temperature, the vial was placed into a 20 mL vial filled with 3 mL of diethyl ether and capped tightly. Upon storing for 2 days, diethyl ether diffused into the stock solution to produce nearly transparent pale-yellow needle-like crystals. Yield: 15 mg (52%). Anal. Calc. for C<sub>18</sub>H<sub>21</sub>Br<sub>3</sub>N<sub>2</sub>OPb (%): C, 29.69; H, 2.91; N, 3.85. Found (%): C, 29.31; H, 2.32; N, 3.14.

**Synthesis of [PyrNH<sub>3</sub>][Pb<sub>2</sub>Br<sub>6</sub>](DMFH)(DMF)<sub>2</sub>.** In a 5 mL scintillation vial filled with 2 mL of DMF, pyren-4-ylmethanamine hydrobromide (15 mg, 0.0383 mmol) was mixed with PbBr<sub>2</sub> (19 mg, 0.0383 mmol) and tetracyanoethylene (4.9 mg, 0.0383 mmol). The resulting suspension was heated until the mixture became clear. After cooling to room temperature, the vial was placed into a 20 mL vial filled with 3 mL of diethyl ether and capped tightly. Upon storing for 2 days, diethyl ether diffused into the stock solution to produce nearly transparent pale-yellow needle-like crystals. Yield: 12 mg (22%). Anal. Calc. for C<sub>26</sub>H<sub>36</sub>Br<sub>6</sub>N<sub>4</sub>O<sub>3</sub>Pb<sub>2</sub> (%): C, 23.19; H, 2.70; N, 4.16. Found (%): C, 22.82; H, 2.42; N, 3.85.

**Synthesis of [StyrNH<sub>3</sub>]<sub>2</sub>[PbBr<sub>4</sub>].** In a 5 mL scintillation vial filled with 2 mL of DMF, (E)-(4-styrylphenyl)methanamine hydrobromide (10 mg, 0.0347 mmol) was mixed with PbBr<sub>2</sub> (12.7 mg, 0.0347 mmol) and tetracyanoethylene (4.4 mg, 0.0347 mmol). The resulting suspension was heated until the mixture became clear. After cooling to room temperature, the vial was placed into a 20 mL vial filled with 3 mL of diethyl ether and capped tightly. Upon storing for 2 days, diethyl ether diffused into the stock solution to produce nearly transparent pale-yellow needle-like crystals. Yield: 5 mg (13%). Anal. Calc. for C<sub>30</sub>H<sub>32</sub>Br<sub>4</sub>N<sub>2</sub>Pb (%): C, 38.03; H, 3.40; N, 2.96. Found (%): C, 37.86; H, 3.12; N, 2.75.

**X-ray crystallography.** X-ray diffraction data for single crystals of [AntrNH<sub>3</sub>][PbBr<sub>3</sub>](DMF) and [StyrNH<sub>3</sub>]<sub>2</sub>[PbBr<sub>4</sub>] were collected at 100 K with a Bruker Quest D8 CCD diffrac-

tometer (Bruker AXS, Karlsruhe, Germany), those for [PyrNH<sub>3</sub>][Pb<sub>2</sub>Br<sub>6</sub>][DMFH](DMF)<sub>2</sub>, at 120 K with a Bruker APEX2 DUO CCD diffractometer (Bruker AXS, Karlsruhe, Germany), both using the graphite monochromated Mo-K $\alpha$  radiation ( $\lambda = 0.71073 \text{ \AA}$ ). Using Olex2 [41], the structures were solved with the ShelXT structure solution program [42] using Intrinsic Phasing and refined with XL refinement package [43] using Least Squares minimization. Hydrogen atoms of NH<sub>3</sub> groups were located in different Fourier synthesis. Positions of other hydrogen atoms were calculated, and they all were refined in the isotropic approximation in the riding model. Disordered solvent molecules of DMF and dichloromethane occupying the same positions in the crystal of [Styr-NH<sub>3</sub>]<sub>2</sub>[PbBr<sub>4</sub>] have been treated as a diffuse contribution to the overall scattering without specific atom positions by SQUEEZE/PLATON [44]. Crystal data and structure refinement parameters are given in Table 1. CCDC 2121268, 2121269 and 2121270 contain the supplementary crystallographic data for [AntrNH<sub>3</sub>][PbBr<sub>3</sub>](DMF), [PyrNH<sub>3</sub>][Pb<sub>2</sub>Br<sub>6</sub>][DMFH](DMF)<sub>2</sub> and [StyrNH<sub>3</sub>]<sub>2</sub>[PbBr<sub>4</sub>], respectively.

**Table 1.** Crystal data and structure refinement parameters for [AntrNH<sub>3</sub>][PbBr<sub>3</sub>](DMF), [PyrNH<sub>3</sub>][Pb<sub>2</sub>Br<sub>6</sub>][DMFH](DMF)<sub>2</sub> and [StyrNH<sub>3</sub>]<sub>2</sub>[PbBr<sub>4</sub>].

Parameter	[AntrNH <sub>3</sub> ][PbBr <sub>3</sub> ](DMF)	[PyrNH <sub>3</sub> ][Pb <sub>2</sub> Br <sub>6</sub> ][DMFH](DMF) <sub>2</sub>	[StyrNH <sub>3</sub> ] <sub>2</sub> [PbBr <sub>4</sub> ]
Formula unit	C <sub>36</sub> H <sub>42</sub> Br <sub>6</sub> N <sub>4</sub> O <sub>2</sub> Pb <sub>2</sub>	C <sub>26</sub> H <sub>36</sub> Br <sub>6</sub> N <sub>4</sub> O <sub>3</sub> Pb <sub>2</sub>	C <sub>30</sub> H <sub>32</sub> Br <sub>4</sub> N <sub>2</sub> Pb
Formula weight	1456.57	1346.43	947.40
T, K	100	120	100
Crystal system	Orthorhombic	Monoclinic	Monoclinic
Space group	P2 <sub>1</sub> 2 <sub>1</sub> 2 <sub>1</sub>	P2 <sub>1</sub> /n	Cc
Z	4	4	16
a, $\text{\AA}$	4.3768(2)	7.5989(7)	22.6541(4)
b, $\text{\AA}$	20.9524(8)	22.120(2)	15.7611(3)
c, $\text{\AA}$	44.9467(15)	22.258(2)	36.9741(7)
$\beta$ , $^\circ$	90	92.060(2)	95.2120(10)
V, $\text{\AA}^3$	4121.8(3)	3738.9(6)	13147.1(4)
$D_{\text{calc}}$ (g cm <sup>-3</sup> )	2.347	2.392	1.915
Linear absorption, $\mu$ (cm <sup>-1</sup> )	140.12	154.37	100.16
F(000)	2704	2472	7168
$2\Theta_{\text{max}}$ , $^\circ$	54	52	54
Reflections measured	85071	36079	200887
Independent reflections	9012	7354	28716
Observed reflections [ $I > 2\sigma(I)$ ]	8637	5245	25396
Parameters	456	376	1260
R1	0.0377	0.0399	0.0500
wR2	0.0843	0.0944	0.1341
GOOF	1.138	1.042	1.039
$\Delta\rho_{\text{max}}/\Delta\rho_{\text{min}}$ (e $\text{\AA}^{-3}$ )	1.620/−1.673	1.972/−1.598	3.283/−1.633

### 3. Results and Discussion

The organic donors (anthracene, pyrene and (E)-stilbene) to form a charge-transfer complex with TCNE were functionalized by a methanamine group to function as organic cations in the hybrid perovskites based on lead(II) bromide. The corresponding hydrobromides AntrNH<sub>3</sub>Br, PyrNH<sub>3</sub>Br and StyrNH<sub>3</sub>Br (Scheme 1) were synthesized in satisfactory yields from related aldehydes by their “one-pot” reductive amination with hydroxyl amine, metal zinc and hydrochloric acid in ethanol and a treatment of the resulting products with hydrobromic acid [40]. Although performing this reaction in two steps gives a 10%-increase in the yield [29], such a “one-pot” procedure facilitates the workup. Anthracene-9-carbaldehyde was obtained by a modified Vilsmeier–Haak procedure [36] (Scheme 2), while 1-pyrenecarbaldehyde, by formylation via lithiation of 1-pyrene bromide and the subsequent reaction with DMF [38,45] (Scheme 3). For (E)-4-styrylbenzaldehyde, a

different approach was used [39], the Heck coupling reaction [39] of 4-bromobenzaldehyde and styrene (Scheme 4).

Each hydrobromide was then dissolved in hot DMF together with  $\text{PbBr}_2$  and TCNE in a ratio of 1:1:1, following a strategy successfully employed to obtain lead bromide-based perovskites with an organic charge-transfer complex between a pyrene donor and 7,7,8,8-tetracyanoquinodimethane (TCNQ) acceptor [21–23]. Attempts to use other high-boiling polar solvents that provided a similarly good solubility of both organic and inorganic reagents (i.e., DMSO and glycerol) produced oily products upon vapor diffusion of diethyl ether into the solutions. In contrast, the crystallization from DMF under the same conditions readily (in a two-day period) resulted in nearly transparent pale-yellow needle-like crystals, which were collected by filtration. We expected them to be new 1D- [21] or 2D- [22,23] hybrid perovskites that contained organic charge-transfer complexes with TCNE; however, the latter was not detected by X-ray diffraction (Figures 1–3). Instead, the obtained crystalline products were perovskitoids [35] with the corresponding methanamonium cations and one-dimensional (1D) or finite arrays of lead bromide octahedra connected via different modes (other than corner-sharing in true perovskites [35]) depending on the polyaromatic/conjugated core in the hydrobromide used.

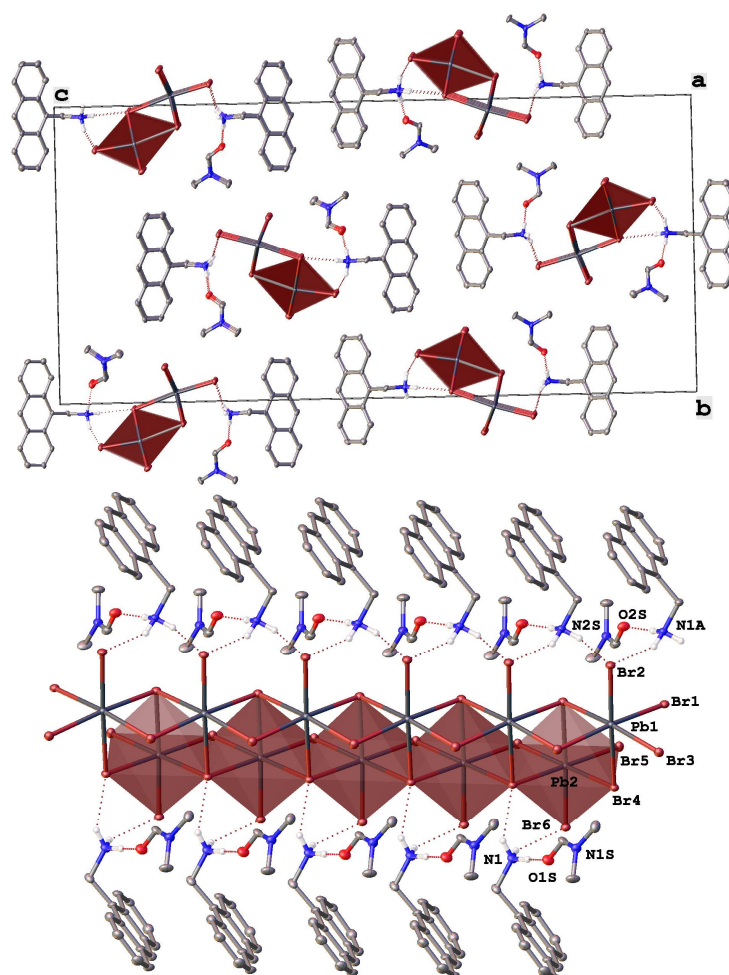


**Figure 1.** Fragments of the crystal packing in  $[\text{AntrNH}_3][\text{PbBr}_3](\text{DMF})$  (**top**) illustrating the formation of 1D ladder-like chains from lead bromide octahedra (highlighted by pink color) along the crystallographic axis *a* and (**bottom**) a view perpendicular to this axis. Hydrogen atoms except those of  $\text{NH}_3$  groups are omitted for clarity, non-hydrogen atoms are shown as thermal ellipsoids ( $p = 30\%$ ) and only labels of the heteroatoms in an asymmetric part of the unit cell are given.

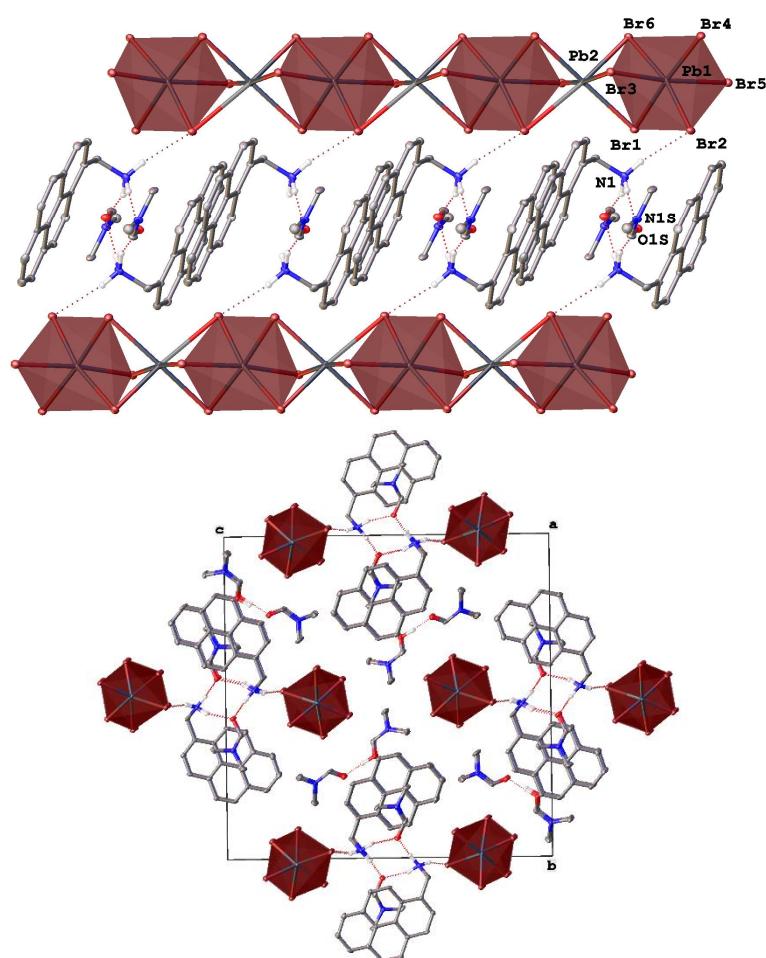


**Figure 2.** Fragments of the crystal packing in  $[\text{PyrNH}_3][\text{Pb}_2\text{Br}_6][\text{DMFH}](\text{DMF})_2$  (**top**) illustrating the formation of 1D-infinite chains from lead bromide octahedra (highlighted by pink color) along the crystallographic axis *a* and (**bottom**) a view perpendicular to this axis. Hydrogen atoms except those of  $\text{NH}_3$  groups are omitted for clarity, non-hydrogen atoms are shown as thermal ellipsoids ( $p = 30\%$ ) and only labels of the heteroatoms in an asymmetric part of the unit cell are given.

Indeed, a new perovskitoid of the composition  $[\text{AntrNH}_3][\text{PbBr}_3](\text{DMF})$  (Figure 1) with two symmetry-independent anthracen-9-ylmethanamonium cations,  $\text{AntrNH}_3^+$ , and two solvent DMF molecules in an asymmetric unit features 1D ladder-like double chains along the crystallographic axis *a* (Figure 1 top) that are made of nearly ideal octahedra, as quantified by a continuous symmetry measure [46] (Table 2), of lead bromide (Pb–Br 2.8402(11)–3.2532(13) Å). Each octahedron is edge-shared to four others in a rare manner found in [47] (Figure 1 bottom).

On the opposite sides, these 1D ladder-like chains are decorated by the organic cations that each form two hydrogen bonds ( $\text{N} \dots \text{Br}$  3.289(11)–3.415(11) Å,  $\text{NHBr}$  131.2(8)–150.0(7)°) via two hydrogen atoms of their ammonium groups. The third atom is H-bonded to the solvent DMF molecule ( $\text{N} \dots \text{O}$  2.767(14) and 2.771(14) Å,  $\text{NHO}$  168.8(7) and 171.3(8)°). In the resulting H-bonded columns, the anthracene cores of the cations are parallel and only 3.419(9) and 3.464(9) Å apart. The  $\pi$ - $\pi$  stacks that they form on each side of the 1D ladder-like chains of lead bromide units in  $[\text{AntrNH}_3][\text{PbBr}_3](\text{DMF})$  run along these chains owing to the ammonium group significantly deviating from the aromatic plane (Figure 1, top); the corresponding angle between the plane and the bond C–N is 115.2(7) and 115.8(7)° in two symmetry-independent cations. Such a packing motif is additionally stabilized by C–H  $\dots$   $\pi$  interactions between the methylene bridges and the anthracene cores of the neighboring cations. The columns are rotated by 78.95(3)° relative to each other (Figure 1, bottom) and are held together only by weak interactions, such as C–H  $\dots$   $\pi$

contacts between the anthracene cores of the cations from the neighboring columns with an angle between their mean planes of  $76.0(3)^\circ$ .

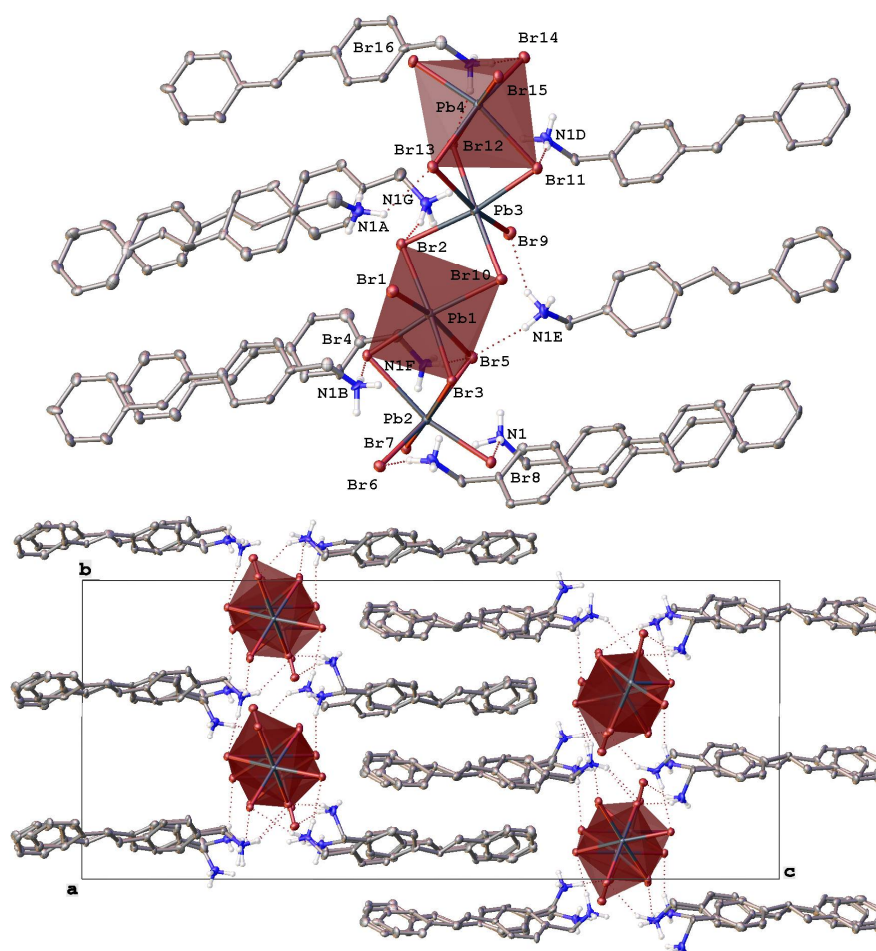


**Figure 3.** Fragments of the crystal packing in  $[\text{StyrNH}_3]_2[\text{PbBr}_4]$  (**top**) illustrating the formation of mini-rods from lead bromide octahedra (highlighted by pink color) along the crystallographic axis a and (**bottom**) a view perpendicular to the crystallographic plane ab. Hydrogen atoms except those of  $\text{NH}_3$  groups are omitted for clarity, non-hydrogen atoms are shown as thermal ellipsoids ( $p = 30\%$ ) and only labels of the heteroatoms in an asymmetric part of the unit cell are given.

**Table 2.** Main geometric parameters and continuous symmetry measures <sup>1</sup> as obtained from X-ray diffraction for  $[\text{AntrNH}_3][\text{PbBr}_3](\text{DMF})$ ,  $[\text{PyrNH}_3][\text{Pb}_2\text{Br}_6][\text{DMFH}](\text{DMF})_2$  and  $[\text{StyrNH}_3]_2[\text{PbBr}_4]$ .

Parameter	$[\text{AntrNH}_3][\text{PbBr}_3](\text{DMF})$	$[\text{PyrNH}_3][\text{Pb}_2\text{Br}_6][\text{DMFH}](\text{DMF})_2$	$[\text{StyrNH}_3]_2[\text{PbBr}_4]$
Pb-Br, Å	2.8480(10)–3.1916(10) [2.8402(11)–3.2532(13)]	2.9250(9)–3.1786(10) [2.8569(9)–3.3482(10)]	2.8717(19)–3.209(2) [2.841(2)–3.225(2), 2.8587(18)–3.232(3), 2.870(2)–3.192(2)]
N ... Br, Å	3.289(11)–3.415(11)	3.537(7)	3.232(14)–3.701(13)
NHBr, °	131.2(8)–150.0(7)°	159.4(4)	119(1)–172(1)
N ... O, Å	2.767(14), 2.771(14)	2.801(9), 2.835(9)	-
NHO, °	168.8(7), 171.3(8)	158.5(4), 163.1(5)	-
O ... O, Å	-	2.42(1)	-
OHO, °	-	166.0(5)	-
$S(\text{O}_h)$	0.122 [0.282]	0.998 [1.138]	0.866 [0.397, 0.885, 0.352]

<sup>1</sup> The values in the brackets are given for other symmetry-independent lead(II) cations;  $S(\text{O}_h)$  is an octahedral symmetry measure, which measures how far is the analyzed polyhedron from a reference shape, the ideal octahedron; for the perfect match,  $S(\text{O}_h) = 0$ .

Using pyren-4-ylmethanamonium hydrobromide  $\text{PyrNH}_3\text{Br}$ , a 1D-hybrid perovskitoid that contains the appropriate cation,  $\text{PyrNH}_3^+$ , and DMF as the lattice solvent was also obtained under the same crystallization conditions. In this case, however, there is another type of organic cations, the protonated DMF species, so that the resulting composition is  $[\text{PyrNH}_3][\text{Pb}_2\text{Br}_6][\text{DMFH}](\text{DMF})_2$  (Figure 2). The 1D-infinite chains along the crystallographic axis  $a$  (Figure 2 top) are made from the lead bromide octahedra (Pb-Br 2.8569(9)–3.3482(10) Å), which are more distorted than in the above 1D-perovskitoid  $[\text{AntrNH}_3][\text{PbBr}_3](\text{DMF})$  as gauged by a continuous symmetry measure (Table 2). Each of them is connected to two other octahedra through a popular face-sharing mode often found in 1D-perovskitoids [12,35] and associated with a significant increase in the band gap [48,49].

Of the bromide anions in  $[\text{PyrNH}_3][\text{Pb}_2\text{Br}_6][\text{DMFH}](\text{DMF})_2$ , only the anion Br(2) that occupies a vertex shared by these octahedra forms a hydrogen bond with the ammonium group of the cation (N . . . Br 3.537(7) Å, NHBr 159.4(4)°). The two other hydrogen atoms are H-bonded to two solvate molecules of DMF (N . . . O 2.801(9) and 2.835(9) Å, NHO 158.5(4) and 163.1(5)°) to produce a centrosymmetric dimer that bridges the above 1D-infinite chains. The other symmetry-independent DMF molecule forms a very strong hydrogen bond with the third, protonated DMF species (O . . . O 2.42(1) Å, OHO 166.0(5)°) that can be, therefore, described as a cation  $[\text{DMF}\cdots\text{H}\cdots\text{DMF}]^+$  with the H-O distances of 0.956(7) and 1.482(7) Å.

In the resulting columns that are decorated from one side by the pyrene cations, the DMF molecules are sandwiched between these cations so that no stacking interactions occur between them; the distance between the centroids of the pyrene core and that of the  $\text{C}_2\text{NCO}$  plane of the DMF molecule tilted by 8.3(3)° is 3.696(4) and 4.411(4) Å. As in the above perovskitoid  $[\text{AntrNH}_3][\text{PbBr}_3](\text{DMF})$ , the stacks of the alternating cations, which feature a similar molecular geometry with the bond C-N to the ammonium group deviating from the aromatic plane by 115.8(4)°, and the DMF molecules run parallel to the 1D-infinite chains. The neighboring columns that are rotated by 90° relative to each other (Figure 2 bottom) are held together through the above centrosymmetric dimers and weaker interactions, such as C-H . . . Br contacts between the lead bromide units and both types of the organic cations, pyren-4-ylmethanamonium  $\text{PyrNH}_3^+$  and the above solvent-derived species  $[\text{DMF}\cdots\text{H}\cdots\text{DMF}]^+$ .

Switching to (E)-(4-styrylphenyl)methanamonium hydrobromide as a source of a potential organic donor that has a very different (elongated) shape from the above “compact” polyaromatic compounds resulted in a completely different, although low-dimensional (0D) [13], perovskitoid material of the composition  $[\text{StyrNH}_3]_2[\text{PbBr}_4]$  (Figure 3). In contrast to  $[\text{AntrNH}_3][\text{PbBr}_3](\text{DMF})$  and  $[\text{PyrNH}_3][\text{Pb}_2\text{Br}_6][\text{DMFH}](\text{DMF})_2$ , it contains finite lead bromide clusters, the mini-rods  $[\text{Pb}_4\text{Br}_{16}]^{8+}$  (Pb-Br 2.606(11)–3.457(13) Å), that run along the crystallographic axis  $a$  parallel to each other (Figure 3 bottom). These mini-rods are made from four lead bromide octahedra that are only slightly distorted (Table 2) and feature yet another binding mode, as they share in the order of a face, an edge and a face (Figure 3 top) similar to an octahedra sharing sometimes found in 1D hybrid perovskitoids [35], such as corner-shared mini-rods in a previously reported bromoplumbate with a N-methylated 4,4'-bipyridine cation [50]. Note that other 0D-perovskitoids often (incorrectly) [51] referred to as 0D-perovskites [13] contain isolated octahedral anions  $\text{MX}_6$  ( $\text{M} = \text{Pb}^{2+}, \text{Sn}^{2+}, \text{Bi}^{3+}$ ;  $\text{X} = \text{Cl}^-, \text{Br}^-, \text{I}^-$ ) or their face-shared dimers [13] or trimers [35].

In  $[\text{StyrNH}_3]_2[\text{PbBr}_4]$ , the mini-rods  $[\text{Pb}_4\text{Br}_{16}]^{8+}$  that can be thought of as two such dimers edge-shared together are decorated and connected by numerous hydrogen bonds with the ammonium groups of the eight symmetry-independent cations (N . . . Br 3.232(14)–3.812(13) Å, NHBr 119(1)–172(1)°) to give H-bonded layers parallel to the crystallographic plane  $ab$ . Within these layers, the mini-rods are additionally connected via halogen bonds (Br . . . Br 2.866(11)–4.230(12) Å) between the bromide anions that assemble them into pseudo-2D arrays of lead bromide octahedra.

The layers are packed into a dense 3D-framework by weak C-H . . .  $\pi$  interactions between the interdigitated 4-styrylphenyl-based cations from the neighboring layers (Figure 3 bottom), thus mirroring a bilayered structure [52] typical of ionic liquid crystals [53] with heterocyclic cations featuring long non-polar alkyl chains. As in the latter case [53], there are no stacking interactions between the conjugated 4-styrylphenyl cores in the bilayers. In contrast, they are nearly perpendicular to each other, which is facilitated by their molecular geometry. Thanks to an elongated shape of the 4-styrylphenyl core, the alkylammonium group does not have to significantly (by 115.2(7)–115.8(7)° in [AntrNH<sub>3</sub>][PbBr<sub>3</sub>](DMF) and [PyrNH<sub>3</sub>][Pb<sub>2</sub>Br<sub>6</sub>][DMFH](DMF)<sub>2</sub>) deviate from the styryl plane to avoid steric hindrances with it. Indeed, the corresponding angle between the bond C-N and this plane varies in a wide range of 17.0(12)–164.7(10)°.

Note that in all cases, the presence of TCNE in the reaction mixture did not stir the outcome towards the above crystalline products, the 1D-hybrid perovskitoids [AntrNH<sub>3</sub>][PbBr<sub>3</sub>](DMF) and [PyrNH<sub>3</sub>][Pb<sub>2</sub>Br<sub>6</sub>][DMFH](DMF)<sub>2</sub> and the pseudo-layered 0D-perovskitoid [54] [StyrNH<sub>3</sub>]<sub>2</sub>[PbBr<sub>4</sub>]. Indeed, omitting it while keeping the same concentrations of lead bromide and the corresponding hydrobromide in DMF, which was the best solvent for this purpose, did not change the result for any of the probed cations. The use of other popular organic acceptors, such as 7,7,8,8-tetracyanoquinodimethane (TCNQ), 1,2,4,5-tetracyanobenzene, hexafluorobenzene, chrolanil or 1,4-benzoquinone, also produced the same 0D- and 1D-hybrid perovskitoids and, sometimes, side-products, such as previously reported [29] lead(II) bromide with DMF PbBr<sub>2</sub>(DMF). Those were also obtained when anti-solvents different from diethyl ether (e.g., dichloromethane or pentane) or other ratios of the reagents were used, such as donor: PbBr<sub>2</sub>: acceptor ratios of 1:1:1, 2:1:1 and 1:1:5.

#### 4. Conclusions

In our search for low-dimensional hybrid perovskites with organic charge-transfer complexes to tune their optoelectronic properties for use in solar cells [21–24,33], new pseudo-layered 0D- and 1D-hybrid perovskitoids [35] (often incorrectly [51] referred to as perovskites) were obtained from lead bromide. They were identified by X-ray diffraction to contain the lead bromide octahedral anions featuring different sharing modes and the alkylammonium cations, the derivatives of aromatic and conjugated molecules common for organic charge-transfer complexes (anthracene, pyrene and (E)-stilbene).

The lack of an organic acceptor may result from steric or electronic effects of the ammonium group that is H-bonded to the lead bromide chains or mini-rods in these 1D- and 0D-hybrid perovskitoids. In the corresponding cations, the ammonium group is separated from the aromatic or conjugated cores only by a methylene bridge, so it may preclude an organic acceptor, even a small TCNE molecule, from approaching these cores or make them electron donors that are not good enough for many other acceptors to form a charge-transfer complex. An experimental piece of evidence is a successful self-assembling of 1D- and 2D-hybrid perovskites under similar conditions by using a functionalized pyrene donor with a longer alkyl chain, pyrene-4-ylbutanamine [21–23].

Although for these reasons we failed to synthesis the low-dimensional hybrid perovskites with organic charge-transfer complexes for solar cells, the obtained 1D-hybrid perovskitoids [AntrNH<sub>3</sub>][PbBr<sub>3</sub>](DMF) and [PyrNH<sub>3</sub>][Pb<sub>2</sub>Br<sub>6</sub>][DMFH](DMF)<sub>2</sub> and the pseudo-layered 0D-perovskitoid [54] [StyrNH<sub>3</sub>]<sub>2</sub>[PbBr<sub>4</sub>] with unusual mini-rods of four face- and edge-shared octahedra can be of use in another type of optoelectronic device, [55,56] photodetectors; [57] testing them for this application is underway in our group.

**Author Contributions:** Conceptualization, Y.V.N.; methodology, K.L.I. and I.A.N.; software, K.L.I. and I.A.N.; validation, I.A.N. and Y.V.N.; formal analysis, K.L.I.; investigation, K.L.I. and I.A.N.; resources, Y.V.N.; data curation, Y.V.N.; writing—original draft preparation, I.A.N. and Y.V.N.; writing—review and editing, Y.V.N.; visualization, K.L.I. and I.A.N.; supervision, Y.V.N.; project administration, Y.V.N.; funding acquisition, Y.V.N. All authors have read and agreed to the published version of the manuscript.

**Funding:** This research was supported by the Russian Foundation for Basic Research (Project 20-33-70052). Elemental analysis was performed using the equipment of the Center for molecular composition studies of INEOS RAS with financial support from the Ministry of Science and Higher Education of the Russian Federation.

**Data Availability Statement:** Not applicable.

**Conflicts of Interest:** The authors declare no conflict of interest.

## References

1. Kojima, A.; Teshima, K.; Shirai, Y.; Miyasaka, T. Organometal halide perovskites as visible-light sensitizers for photovoltaic cells. *J. Am. Chem. Soc.* **2009**, *131*, 6050–6051. [[CrossRef](#)]
2. Chouhan, L.; Ghimire, S.; Subrahmanyam, C.; Miyasaka, T.; Biju, V. Synthesis, optoelectronic properties and applications of halide perovskites. *Chem. Soc. Rev.* **2020**, *49*, 2869–2885. [[CrossRef](#)] [[PubMed](#)]
3. Liu, C.; Hu, M.; Zhou, X.; Wu, J.; Zhang, L.; Kong, W.; Li, X.; Zhao, X.; Dai, S.; Xu, B.; et al. Efficiency and stability enhancement of perovskite solar cells by introducing CsPbI<sub>3</sub> quantum dots as an interface engineering layer. *NPG Asia Mater.* **2018**, *10*, 552–561. [[CrossRef](#)]
4. Huo, C.; Cai, B.; Yuan, Z.; Ma, B.; Zeng, H. Two-Dimensional Metal Halide Perovskites: Theory, Synthesis, and Optoelectronics. *Small Methods* **2017**, *1*, 1600018. [[CrossRef](#)]
5. Smith, I.C.; Hoke, E.T.; Solis-Ibarra, D.; McGehee, M.D.; Karunadasa, H.I. A Layered Hybrid Perovskite Solar-Cell Absorber with Enhanced Moisture Stability. *Angew. Chem. Int. Ed.* **2014**, *53*, 11232–11235. [[CrossRef](#)] [[PubMed](#)]
6. Zhou, C.; Worku, M.; Neu, J.; Lin, H.; Tian, Y.; Lee, S.; Zhou, Y.; Han, D.; Chen, S.; Hao, A.; et al. Facile Preparation of Light Emitting Organic Metal Halide Crystals with Near-Unity Quantum Efficiency. *Chem. Mat.* **2018**, *30*, 2374–2378. [[CrossRef](#)]
7. Saparov, B.; Mitzi, D.B. Organic–Inorganic Perovskites: Structural Versatility for Functional Materials Design. *Chem. Rev.* **2016**, *116*, 4558–4596. [[CrossRef](#)]
8. Kieslich, G.; Sun, S.; Cheetham, A.K. An extended Tolerance Factor approach for organic–inorganic perovskites. *Chem. Sci.* **2015**, *6*, 3430–3433. [[CrossRef](#)] [[PubMed](#)]
9. Travis, W.; Glover, E.N.K.; Bronstein, H.; Scanlon, D.O.; Palgrave, R.G. On the application of the tolerance factor to inorganic and hybrid halide perovskites: A revised system. *Chem. Sci.* **2016**, *7*, 4548–4556. [[CrossRef](#)]
10. Grancini, G.; Nazeeruddin, M.K. Dimensional tailoring of hybrid perovskites for photovoltaics. *Nat. Rev. Mater.* **2019**, *4*, 4–22. [[CrossRef](#)]
11. Mousdis, G.A.; Gionis, V.; Papavassiliou, G.C.; Raptopoulou, C.P.; Terzis, A. Preparation, structure and optical properties of [CH<sub>3</sub>SC(=NH<sub>2</sub>)NH<sub>2</sub>]<sub>3</sub>PbI<sub>5</sub>, [CH<sub>3</sub>SC(=NH<sub>2</sub>)NH<sub>2</sub>]<sub>4</sub>Pb<sub>2</sub>Br<sub>8</sub> and [CH<sub>3</sub>SC(=NH<sub>2</sub>)NH<sub>2</sub>]<sub>3</sub>PbCl<sub>5</sub>·CH<sub>3</sub>SC(=NH<sub>2</sub>)NH<sub>2</sub>Cl. *J. Mat. Chem.* **1998**, *8*, 2259–2262. [[CrossRef](#)]
12. Rahaman, M.Z.; Ge, S.; Lin, C.-H.; Cui, Y.; Wu, T. One-Dimensional Molecular Metal Halide Materials: Structures, Properties, and Applications. *Small Struct.* **2021**, *2*, 2000062. [[CrossRef](#)]
13. Sun, S.; Lu, M.; Gao, X.; Shi, Z.; Bai, X.; Yu, W.W.; Zhang, Y. 0D Perovskites: Unique Properties, Synthesis, and Their Applications. *Adv. Sci.* **2021**, 2102689. [[CrossRef](#)] [[PubMed](#)]
14. Zhou, C.; Lin, H.; Lee, S.; Chaaban, M.; Ma, B. Organic–inorganic metal halide hybrids beyond perovskites. *Mat. Res. Lett.* **2018**, *6*, 552–569. [[CrossRef](#)]
15. Passarelli, J.V.; Fairfield, D.J.; Sather, N.A.; Hendricks, M.P.; Sai, H.; Stern, C.L.; Stupp, S.I. Enhanced Out-of-Plane Conductivity and Photovoltaic Performance in n = 1 Layered Perovskites through Organic Cation Design. *J. Am. Chem. Soc.* **2018**, *140*, 7313–7323. [[CrossRef](#)]
16. Evans, H.A.; Lehner, A.J.; Labram, J.G.; Fabini, D.H.; Barreda, O.; Smock, S.R.; Wu, G.; Chabiny, M.L.; Seshadri, R.; Wudl, F. (TTF)Pb<sub>2</sub>I<sub>5</sub>: A Radical Cation-Stabilized Hybrid Lead Iodide with Synergistic Optoelectronic Signatures. *Chem. Mater.* **2016**, *28*, 3607–3611. [[CrossRef](#)]
17. Maughan, A.E.; Kurzman, J.A.; Neilson, J.R. Hybrid inorganic-organic materials with an optoelectronically active aromatic cation: (C<sub>7</sub>H<sub>7</sub>)<sub>2</sub>SnI<sub>6</sub> and C<sub>7</sub>H<sub>7</sub>PbI<sub>3</sub>. *Inorg. Chem.* **2015**, *54*, 370–378. [[CrossRef](#)]
18. Van Gompel, W.T.M.; Herckens, R.; Denis, P.-H.; Mertens, M.; Gélvez-Rueda, M.C.; Van Hecke, K.; Ruttens, B.; D’Haen, J.; Grozema, F.C.; Lutsen, L.; et al. 2D layered perovskite containing functionalised benzothieno-benzothiophene molecules: Formation, degradation, optical properties and photoconductivity. *J. Mater. Chem. C* **2020**, *8*, 7181–7188. [[CrossRef](#)]
19. Pious, J.K.; Basavarajappa, M.G.; Muthu, C.; Krishna, N.; Nishikubo, R.; Saeki, A.; Chakraborty, S.; Vijayakumar, C. Anisotropic Photoconductivity and Long-Lived Charge Carriers in Bismuth-Based One-Dimensional Perovskite with Type-IIa Band Alignment. *J. Phys. Chem. Lett.* **2020**, *11*, 6757–6762. [[CrossRef](#)]
20. Lédée, F.; Audebert, P.; Trippé-Allard, G.; Galmiche, L.; Garrot, D.; Marrot, J.; Lauret, J.-S.; Deleporte, E.; Katan, C.; Even, J.; et al. Tetrazine molecules as an efficient electronic diversion channel in 2D organic–inorganic perovskites. *Mater. Horiz.* **2021**, *8*, 1547–1560. [[CrossRef](#)]
21. Marchal, N.; Van Gompel, W.; Gélvez-Rueda, M.C.; Vandewal, K.; Van Hecke, K.; Boyen, H.-G.; Conings, B.; Herckens, R.; Maheshwari, S.; Lutsen, L.; et al. Lead-Halide Perovskites Meet Donor–Acceptor Charge-Transfer Complexes. *Chem. Mater.* **2019**, *31*, 6880–6888. [[CrossRef](#)]

22. Van Gompel, W.T.M.; Herckens, R.; Van Hecke, K.; Ruttens, B.; D'Haen, J.; Lutsen, L.; Vanderzande, D. Towards 2D layered hybrid perovskites with enhanced functionality: Introducing charge-transfer complexes via self-assembly. *Chem. Commun.* **2019**, *55*, 2481–2484. [[CrossRef](#)]
23. Gélvez-Rueda, M.C.; Van Gompel, W.T.M.; Herckens, R.; Lutsen, L.; Vanderzande, D.; Grozema, F.C. Inducing Charge Separation in Solid-State Two-Dimensional Hybrid Perovskites through the Incorporation of Organic Charge-Transfer Complexes. *J. Phys. Chem. Lett.* **2020**, *11*, 824–830. [[CrossRef](#)] [[PubMed](#)]
24. Li, M.-H.; You, M.-H.; Lin, M.-J. Encapsulating third donors into D–A hybrid heterostructures to form three-component charge-transfer complexes for enhanced electrical properties. *Dalton Trans.* **2021**, *50*, 13961–13967. [[CrossRef](#)] [[PubMed](#)]
25. Milić, J.V. Multifunctional layered hybrid perovskites. *J. Mater. Chem. C* **2021**, *9*, 11428–11443. [[CrossRef](#)]
26. Goetz, K.P.; Vermeulen, D.; Payne, M.E.; Kloc, C.; McNeil, L.E.; Jurchescu, O.D. Charge-transfer complexes: New perspectives on an old class of compounds. *J. Mat. Chem. C* **2014**, *2*, 3065–3076. [[CrossRef](#)]
27. Jiang, H.; Hu, P.; Ye, J.; Zhang, K.K.; Long, Y.; Hu, W.; Kloc, C. Tuning of the degree of charge transfer and the electronic properties in organic binary compounds by crystal engineering: A perspective. *J. Mat. Chem. C* **2018**, *6*, 1884–1902. [[CrossRef](#)]
28. Shen, D.; Chen, W.-C.; Lo, M.-F.; Lee, C.-S. Charge-transfer complexes and their applications in optoelectronic devices. *Mater. Today Energy* **2021**, *20*, 100644. [[CrossRef](#)]
29. Isakovskaya, K.L.; Nikovskii, I.A.; Nelyubina, Y.V. New Low-Dimensional Perovskites Based on Lead Bromide. *Russ. J. Coord. Chem.* **2021**, *47*, 365–375. [[CrossRef](#)]
30. Hashidzume, A.; Zheng, Y.; Takashima, Y.; Yamaguchi, H.; Harada, A. Macroscopic Self-Assembly Based on Molecular Recognition: Effect of Linkage between Aromatics and the Polyacrylamide Gel Scaffold, Amide versus Ester. *Macromolecules* **2013**, *46*, 1939–1947. [[CrossRef](#)]
31. Yuan, Y.; Yan, X.-S.; Li, X.-R.; Cao, J.-L.; Li, Z.; Jiang, Y.-B. Folded short azapeptide for conformation switching-based fluorescence sensing. *Chem. Commun.* **2017**, *53*, 13137–13140. [[CrossRef](#)]
32. Murugesan, K.; Beller, M.; Jagadeesh, R.V. Reusable Nickel Nanoparticles-Catalyzed Reductive Amination for Selective Synthesis of Primary Amines. *Angew. Chem. Int. Ed.* **2019**, *58*, 5064–5068. [[CrossRef](#)]
33. Zhang, F.; Lu, H.; Tong, J.; Berry, J.J.; Beard, M.C.; Zhu, K. Advances in two-dimensional organic–inorganic hybrid perovskites. *Energy Environ. Sci.* **2020**, *13*, 1154–1186. [[CrossRef](#)]
34. Mitzi, D.B.; Liang, K.; Wang, S. Synthesis and Characterization of  $[\text{NH}_2\text{C}(\text{I})\text{NH}_2]_2\text{ASnI}_5$  with A = Iodoformamidinium or Formamidinium: The Chemistry of Cyanamide and Tin(II) Iodide in Concentrated Aqueous Hydriodic Acid Solutions. *Inorg. Chem.* **1998**, *37*, 321–327. [[CrossRef](#)]
35. Wong, W.P.D.; Hanna, J.V.; Grimsdale, A.C. The classification of 1D ‘perovskites’. *Acta Cryst. B* **2020**, *77*, 408–415. [[CrossRef](#)] [[PubMed](#)]
36. Fieser, L.F.; Hartwell, J.L.; Jones, J.E. 9-Anthraldehyde; 2-Ethoxy-1-Naphthaldehyde. *Org. Synth.* **1940**, *20*, 11.
37. Chidirala, S.; Ulla, H.; Valaboju, A.; Kiran, M.R.; Mohanty, M.E.; Satyanarayan, M.N.; Umesh, G.; Bhanuprakash, K.; Rao, V.J. Pyrene–Oxadiazoles for Organic Light-Emitting Diodes: Triplet to Singlet Energy Transfer and Role of Hole-Injection/Hole-Blocking Materials. *J. Org. Chem.* **2016**, *81*, 603–614. [[CrossRef](#)] [[PubMed](#)]
38. Schulze, M.; Scherer, A.; Diner, C.; Tykwinski, R.R. Synthesis of 1-Bromopyrene and 1-Pyrenecarbaldehyde. *Org. Synth.* **2016**, *93*, 100–114. [[CrossRef](#)]
39. Yao, Q.; Kinney, E.P.; Yang, Z. Ligand-Free Heck Reaction:  $\text{Pd}(\text{OAc})_2$  as an Active Catalyst Revisited. *J. Org. Chem.* **2003**, *68*, 7528–7531. [[CrossRef](#)]
40. Ayedi, M.A.; Le Bigot, Y.; Ammar, H.; Abid, S.; Gharbi, R.E.; Delmas, M. Synthesis of Primary Amines by One-Pot Reductive Amination of Aldehydes. *Synth. Commun.* **2013**, *43*, 2127–2133. [[CrossRef](#)]
41. Dolomanov, O.V.; Bourhis, L.J.; Gildea, R.J.; Howard, J.A.K.; Puschmann, H. OLEX2: A Complete Structure Solution, Refinement and Analysis Program. *J. Appl. Cryst.* **2009**, *42*, 339–341. [[CrossRef](#)]
42. Sheldrick, G.M. SHELXT—Integrated space-group and crystal-structure determination. *Acta Cryst. A* **2015**, *71*, 3–8. [[CrossRef](#)]
43. Sheldrick, G.M. Crystal structure refinement with SHELXL. *Acta Cryst. C* **2015**, *71*, 3–8. [[CrossRef](#)] [[PubMed](#)]
44. Spek, A.L. Structure validation in chemical crystallography. *Acta Cryst. D* **2009**, *65*, 148–155. [[CrossRef](#)]
45. Jones, G.B.; Mathews, J.E. Bifunctional antitumor agents. Derivatives of pyrrolo[9,10-b]phenanthrene—A DNA intercalative delivery template. *Tetrahedron* **1997**, *53*, 14599–14614. [[CrossRef](#)]
46. Alvarez, S. Distortion Pathways of Transition Metal Coordination Polyhedra Induced by Chelating Topology. *Chem. Rev.* **2015**, *115*, 13447–13483. [[CrossRef](#)]
47. Eppel, S.; Fridman, N.; Frey, G. Amide-Templated Iodoplumbates: Extending Lead-Iodide Based Hybrid Semiconductors. *Cryst. Growth Des.* **2015**, *15*, 4363–4371. [[CrossRef](#)]
48. Kamminga, M.E.; de Wijs, G.A.; Havenith, R.W.A.; Blake, G.R.; Palstra, T.T.M. The Role of Connectivity on Electronic Properties of Lead Iodide Perovskite-Derived Compounds. *Inorg. Chem.* **2017**, *56*, 8408–8414. [[CrossRef](#)]
49. Mao, L.; Guo, P.; Kepenekian, M.; Hadar, I.; Katan, C.; Even, J.; Schaller, R.D.; Stoumpos, C.C.; Kanatzidis, M.G. Structural Diversity in White-Light-Emitting Hybrid Lead Bromide Perovskites. *J. Am. Chem. Soc.* **2018**, *140*, 13078–13088. [[CrossRef](#)]
50. Liu, G.; Liu, J.; Tao, X.; Li, D.-S.; Zhang, Q. Surfactants as additives make the structures of organic–inorganic hybrid bromoplumbates diverse. *Inorg. Chem. Front.* **2016**, *3*, 1388–1392. [[CrossRef](#)]
51. Akkerman, Q.A.; Manna, L. What Defines a Halide Perovskite? *ACS Energy Lett.* **2020**, *5*, 604–610. [[CrossRef](#)] [[PubMed](#)]

52. Getsis, A.; Mudring, A.V. Imidazolium based ionic liquid crystals: Structure, photophysical and thermal behaviour of C(n)mim Br center dot xH(2)O (n = 12, 14; x = 0, 1). *Cryst. Res. Technol.* **2008**, *43*, 1187–1196. [[CrossRef](#)]
53. Binnemans, K. Ionic liquid crystals. *Chem. Rev.* **2005**, *105*, 4148–4204. [[CrossRef](#)]
54. Mao, L.; Stoumpos, C.C.; Kanatzidis, M.G. Two-Dimensional Hybrid Halide Perovskites: Principles and Promises. *J. Am. Chem. Soc.* **2019**, *141*, 1171–1190. [[CrossRef](#)] [[PubMed](#)]
55. Feng, J.; Gong, C.; Gao, H.; Wen, W.; Gong, Y.; Jiang, X.; Zhang, B.; Wu, Y.; Wu, Y.; Fu, H.; et al. Single-crystalline layered metal-halide perovskite nanowires for ultrasensitive photodetectors. *Nat. Electron.* **2018**, *1*, 404–410. [[CrossRef](#)]
56. Tang, Y.; Liang, M.; Chang, B.; Sun, H.; Zheng, K.; Pullerits, T.; Chi, Q. Lead-free double halide perovskite Cs<sub>3</sub>BiBr<sub>6</sub> with well-defined crystal structure and high thermal stability for optoelectronics. *J. Mat. Chem. C* **2019**, *7*, 3369–3374. [[CrossRef](#)]
57. García de Arquer, F.P.; Armin, A.; Meredith, P.; Sargent, E.H. Solution-processed semiconductors for next-generation photodetectors. *Nat. Rev. Mat.* **2017**, *2*, 16100. [[CrossRef](#)]